CrossMark

The influence of an abandoned goaf on surface subsidence in an adjacent working coal face: a prediction method

Huaizhan Li[1,2] · Binchen Zhao[1,2,3] · Guangli Guo[1,2] · Jianfeng Zha[1,2] · Jingxue Bi[1,2]

Abstract Historical global coal resource exploitation has resulted in goaf abandonment at most mines, which, during the life of the mine, exerts a strong influence on the ability to exploit new working faces adjacent to any abandoned goaf. Thus, the distribution law of the surface subsidence basin above the new working face differs from the general law. Given the lack of research on this distribution law, this study uses a similar material simulation method to examine the influencing mechanism(s) of abandoned goafs on the subsidence basin in the same coal seam. Synthetic aperture radar (SAR) monitoring results of the 9310 working face in the Nan Tun coal mine, Yanzhou, China, are used to verify analytical results, followed by numerical simulation to study the influence of the abandoned goaf on the subsidence basin. Finally, to accurately predict surface subsidence influenced by the abandoned goaf, inflection point deviations are selected and discussed in terms of the probability integral method. This allows for prediction of the distribution of the surface subsidence basin, and moreover, the predicted results are found to be consistent with the SAR monitoring results when the derivation of inflection points is revised.

Keywords Surface subsidence · Goaf · Coal seam · Inflection point · SAR

Introduction

Underground mining can cause various environmental and geological hazards that can affect the environment and safety of a mining area. One of the main hazards is surface subsidence, which is mainly studied in terms of the position and value of a surface subsidence basin. To help reduce and possibly solve the problems of surface subsidence and to evaluate the degree of damage to buildings and other structural in an area, many scholars have studied the distribution of such a surface subsidence basin. For example, Liu and Liao (1965) developed Litwiniszyn's Random Medium Theory and put forward a probability integration method for mining subsidence prediction. Also, Yang et al. (2011) studied the dynamic changes in the surface subsidence basin based on rheological theory. Liu and Cao (2012) applied plate theory to establish mechanical models of surface subsidence in inclined seams by assuming that the bending zone is the key stratum closest to the surface, thus controlling the final form of the surface subsidence basin. It was found that the surface subsidence was far less than the thickness of the stratum. Guo et al. (2004) put forward a subsidence prediction model for non-full mining based on a probability density function method, and Yin et al. (2010) used a surface fitting method to fit mining space and predict mining subsidence. Nie et al. (2015) developed a surface subsidence prediction model based on an arc-tangent function. After comparing the surface

✉ Huaizhan Li
lh_zhan@163.com

1 School of Environment Science and Spatial Informatics, China University of Mining and Technology, Xuzhou 221116, Jiangsu, China

2 NASG Key Laboratory of Land Environment and Disaster Monitoring, China University of Mining and Technology, Xuzhou, China

3 School of Civil Engineering, Shandong Jiaotong University, Jinan 250031, Shandong, China

subsidence characteristics between gasification strip mining and strip mining, Li et al. (2015) proposed a surface subsidence prediction method for underground coal gasification. Guo et al. (2014) put forward a surface subsidence prediction method for backfill mining based on equivalent mining height theory, and Soni et al. (2007) used the profile function method to predict surface subsidence of inclined seams. Baryakh et al. (2005) established a dynamic surface subsidence prediction method that accounts for time and Nicieza et al. (2005) used a three-dimensional (3-D) n–k–g influencing function to predict surface subsidence. So far, the probability integral method has been widely used to predict surface subsidence in practical engineering applications (Li et al. 2007; Yang et al. 2007; Gu and Hong 2012; Wu et al. 2010; Gu et al. 2011). The basis of the method is that the maximum value of surface subsidence is in the center of the goaf during horizontal coal mining and shifts to a downhill direction during inclined coal mining; the contour lines of surface subsidence are concentric rings centered on the area of maximum subsidence. This does, however, only apply to just a single working face. The mining of a new working face will be influenced by one or more adjacent, abandoned goafs, and it has been found that the predicted results of surface subsidence differ significantly from actual results, which can lead to underestimation of the potential damage to surrounding infrastructure and seriously threaten the safety of mining operations.

As a result, this paper presents results of studying the distribution law of surface subsidence that is influenced by an abandoned goaf. The influencing mechanism(s) on the same, adjacent coal seam are first analyzed, and a second set of synthetic aperture radar (SAR) monitoring data of the 9310 working coal face in the Nan Tun mine, Yanzhou, China, are used to verify the analysis. A numerical simulation method is applied to study the law(s) of influence of the abandoned goaf. The results of this study provide an important reference point for the improvement of surface subsidence prediction, as well as in practical engineering applications.

Analysis of surface subsidence distribution

Similar material experiment

To study the influence of abandoned goafs on surface subsidence, it is necessary to understand the overlying strata morphology and structure. To do this, a similar material model is established at constant temperature and humidity. Similar material simulation reduces the size of the mine at a fixed ratio according to the similarity principle. Coal mining is then simulated in the model, and overlying strata are observed for movement and damage. Finally, the actual strata are analyzed according to the conditions in the model to develop predictions based on the characteristics observed (He et al. 1991). This model uses the 9310 working face of the Nan Tun coal mine as an example, and in the experiment, river sand and mica powder are the raw materials, with gypsum and calcium carbonate being used as cementing materials. Mica plates are laid between layers to represent joint effects. The experimental materials and their ratios are listed in Table 1.

The dimensions of the model are $3000 \times 300 \times 1100$ mm. To eliminate boundary effects, a 1000 mm boundary is reserved on the sides of the model. The excavation length is 1000 mm, and it is excavated 20 times; the excavation is located in the middle of the model. Figure 1 shows the morphology and structure of the overlying strata of the similar material model after excavation.

The compaction characteristics of rock caving are markedly divided from the boundary of the goaf to the center in the model. This is because of the bearing effect of the voussoir beam and cantilever structures. The void region is mainly located near the open-off cut and mining stop line. The compaction area is located in the middle of the goaf, and the under-compacted area is in transition between the void and compaction regions. The mining activities around the abandoned goaf are bound to influence the overlying strata morphology and structure of the

Table 1 Experimental materials and their ratios

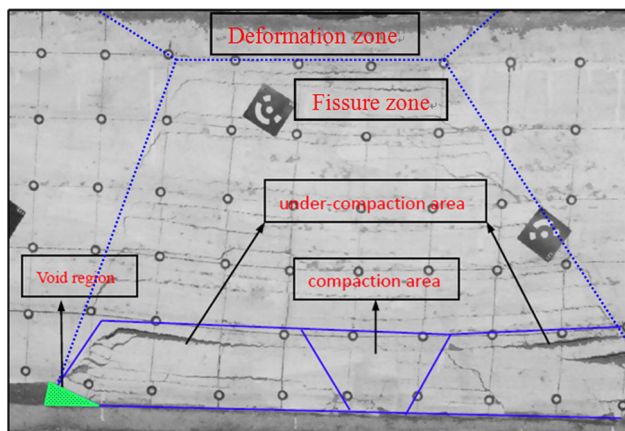| Lithology	Ratio	Sand	Mica	Gypsum	Calcium carbonate
Baseboard (fine sandstone)	71:13:16 (7:3)	80.75	3.25	11.2	4.8
Coal	80:17:3 (7:3)	92.75	4.25	2.1	0.9
Sandy mudstone interbed	71:23:6 (3:7)	88.25	5.75	1.8	4.2
Siltstone	79:16:5 (5:5)	91	4	2.5	2.5
Fine sandstone	74:16:10 (5:5)	86	4	5	5
Fine silts stone interbed	74:16:10 (3:7)	86	4	3	7
Weathered mudstone	73:23:4 (5:5)	90.25	5.75	2	2
Surface soil layer	80:18:2 (3:7)	93.5	4.5	0.6	1.4

Fig. 1 Overlying strata morphology and structure after excavation of the similar material model
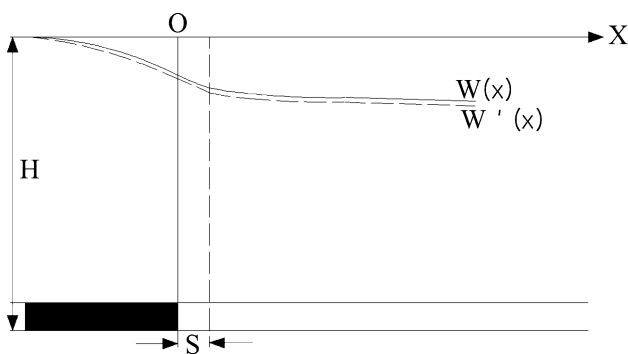

Fig. 2 Ideal and actual subsidence above the goaf

abandoned goaf, especially with respect to the void region and under-compacted area.

Theoretical analysis of the abandoned goaf

Assuming that all of the mining-induced fractures were fully filled and compressed after overlying strata movement, the surface movement basin should be an ideal random medium model. The ideal and limiting surface subsidence distribution $W'(x)$ is shown in Fig. 2.

The limiting subsidence distribution curve $W'(x)$ of half-infinite mining is given as follows:

$$W'(x) = \frac{q'm}{2}\left[erf\left(\frac{\sqrt{\pi}}{r}x\right) + 1\right], \tag{1}$$

where $W'(x)$ is the subsidence curve of an ideal random medium model, m is the mining thickness, q' is the limiting subsidence coefficient ($q' > q$), R is the major influence radius, and x is the distance to the mined-out area boundary. In practice, and because of the broken rock mass and inadequate roof caving, the actual surface subsidence curve is given by:

$$W(x) = \frac{qm}{2}\left[erf\left(\frac{\sqrt{\pi}}{r}(x - s)\right) + 1\right], \tag{2}$$

where $W(x)$ is the subsidence curve of the actual random medium model, m is the mining thickness, q is the subsidence coefficient, and S is the inflection point offset. Under the influence of adjacent working face, the inflection point offset of the abandoned goaf decreases. Therefore, the surface subsidence value of the abandoned goaf will increase. Meanwhile, the inflection point offset of the adjacent working face also decreases under the influence of the abandoned goaf. Thus, the surface subsidence value of the adjacent working face also increases and the change in inflection point offset of the abandoned goaf and adjacent working face will lead to an offset in the distribution of the surface subsidence basin above the working face.

Mechanism of influence for the abandoned goaf

Figure 3 shows a schematic diagram of the influence of the abandoned goaf on the distribution of the surface subsidence basin. When the working face is close to the abandoned goaf, surface subsidence refers to the new mining-induced surface subsidence and residual subsidence of the abandoned goaf. Moreover, the working face mining may cause instability of the masonry beam structure on the boundary of the abandoned goaf. The void region on the boundary may be filled by caved rocks, thus causing secondary subsidence of the goaf. The secondary subsidence will affect the distribution and value of surface subsidence, and the compaction of fractured rock mass in the boundary and middle of the abandoned goaf will increase during the working face mining process, thereby increasing secondary surface subsidence in the abandoned goaf. When the working face is far from the abandoned goaf, the abandoned goaf does not necessarily influence the working face mining, and secondary subsidence may not occur. In turn, the secondary subsidence has little or no effect on the distribution and value of surface subsidence.

Based on the above analysis, the distribution of the surface subsidence basin is related to the distance between the working face and the abandoned goaf. When the distance is small, the partition coal pillars in the middle, or the rock mass, become unstable, and the masonry beam structure on the boundary of the abandoned goaf also becomes unstable. At this time, the abandoned goaf has the greatest influence on surface subsidence above the working face.

When the distance is large, the partition coal pillars are stable and no instability of the masonry beam structure is caused. At this time, the effect of the abandoned goaf on surface subsidence is limited. When the distance is great,
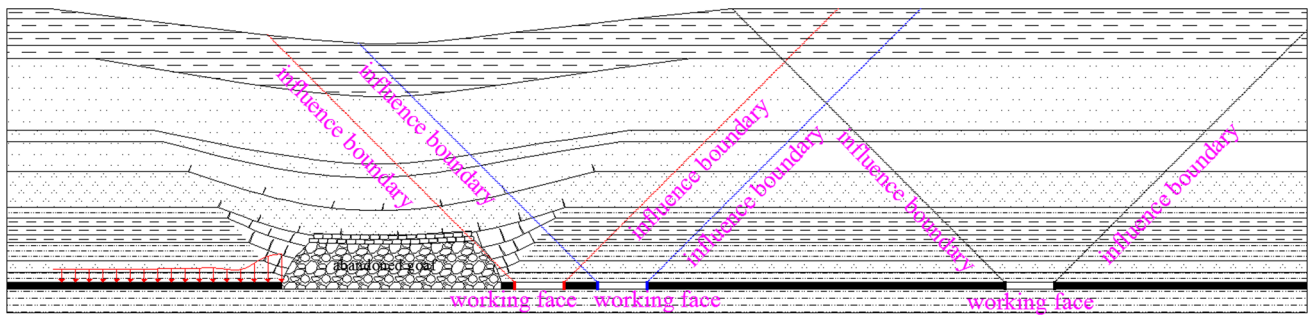
Fig. 3 Schematic diagram showing the influence of the abandoned goaf on surface subsidence basin distribution

the partition coal pillars are stable, and working face mining will not generate additional stress on the abandoned goaf. The surface subsidence basin will also not be affected by the abandoned goaf.

Thus, there are two critical values of influence by the abandoned goaf: one is the distance between the working face and the abandoned goaf when the partition coal pillars or the rock mass are in a stable state, and the other is the distance between the working face and the abandoned goaf, when new working face mining does not generate additional stress on the abandoned goaf. The first critical value can be fixed empirically by the coal pillar instability, similar material simulation or numerical simulation. The second critical value can be fixed according to the mine boundary angle, similar material simulation or the numerical simulation method.

Overlying strata will tend to form small stress arches; thus the degree of caving rock and rock strata compaction will be limited when mining is limited, and when mining increases, the stress arches of the overlying strata will become unstable (Zhang 2009). This increases the degree of rock caving and compaction of middle strata. Also, when the width of the abandoned goaf is limited, the compaction of middle caved strata will be limited, and when the working face is close to the abandoned goaf, additional stress will be generated and compaction of the middle fractured rock mass in the goaf will increase. Conversely, when the width of the abandoned goaf is large, compaction of the middle fractured rock mass increases. Thus, the width of the abandoned goaf greatly affects the distribution of the surface subsidence basin above the adjacent working face.

Study area and D-InSAR monitoring

Study area

The 9310 working face is located in No. 9 mining area of the Nan Tun coal mine (Fig. 4). The coal seam is found in Permo-Carboniferous strata, which are overlain by 111 m
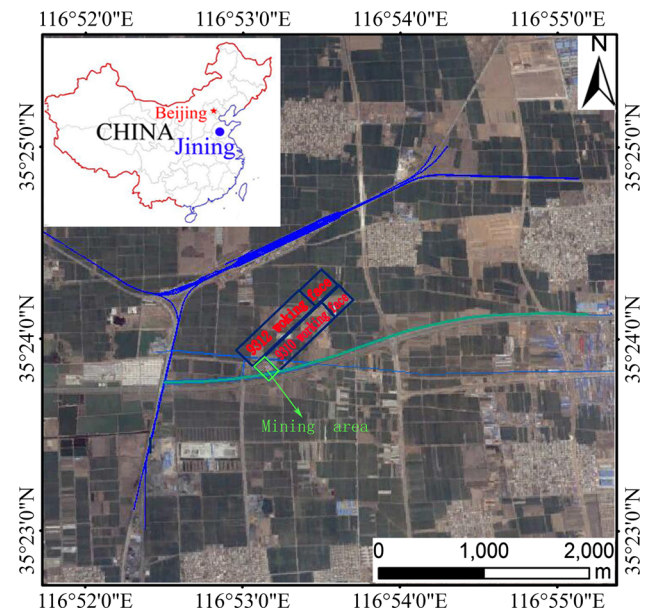

Fig. 4 Location of the Nan Tun coal mine, Yanzhou

of Quaternary strata. During the monitoring period, the upper seam of the No. 3 coal seam of the 9310 working face was being excavated. At this time, the upper seam of the No. 3 coal seam of 9312 working face was being mined. The average thickness of the upper seam is 5 m, and dips at 9°. Fully mechanized top coal caving mining and full-seam mining have been adopted in this mine. Figure 5 shows a schematic diagram of the working face in the No. 9 mining area.

D-InSAR monitoring and data sources

Differential SAR interferometry (D-InSAR) is a micro-wave remote sensing technology for large area micro-deformation monitoring. It uses complex SAR interference at different times provided by SAR to obtain interferograms and surface deformation in targeted areas after differential processing. The precision can reach centimeter level (Fan 2010), and it overcomes some limitations of conventional discrete point observation, such as total stations and GPS.
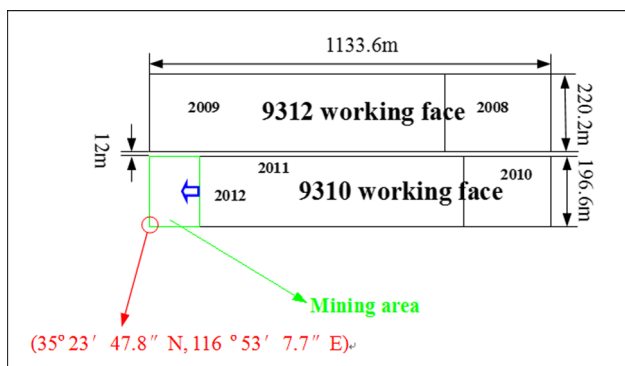
Fig. 5 Schematic diagram showing the working faces of the No. 9 mining area at the same mining level

The use of D-InSAR can help to accurately measure the deformation region and deformation development.

The common D-InSAR data processing methods include the two-pass method (Gabriel et al. 1989), the three-rail method, the four-rail method, and time series PS-InSAR (persistent scatterer InSAR). The two-pass method was used in this study to allow for correct interpretation of subsidence and deformation of the 9310 working face in the study area. The basic principle applied is to use SAR images obtained before and after surface deformation to create interference fringe patterns (including deformation phase and topography phase). Then, existing digital elevation model (DEM) data is used for topographic phase simulation. Finally, the surface deformation is obtained by removing the topography from the interference fringe pattern.

To study the deformation of the 9310 working face in terms of subsidence, deformation and development, ten SAR images were obtained from the TerraSAR-X satellite (3 m resolution) and Shuttle Radar Topography Mission (SRTM) (Zebker and Goldstein 1986). The DEM data, with 90 m resolution, were obtained from the European Space Agency (ESA).

Data processing and results of D-InSAR

Image sets were selected after two-pass filtering of the SAR differential inference processing. This image set was then benchmarked against two consecutive images; the related image sets and parameters are listed in Table 2.

Nine deformation maps of time series between December 25, 2011, and April 2, 2012, were obtained. To intuitively and accurately overlay other spatial information and show the dynamic development of the 9310 working face surface deformation, the deformation maps were processed with Geographic Information Systems (GIS) technology. Figure 6 shows the deformation maps of the 9310 working face in a time series.
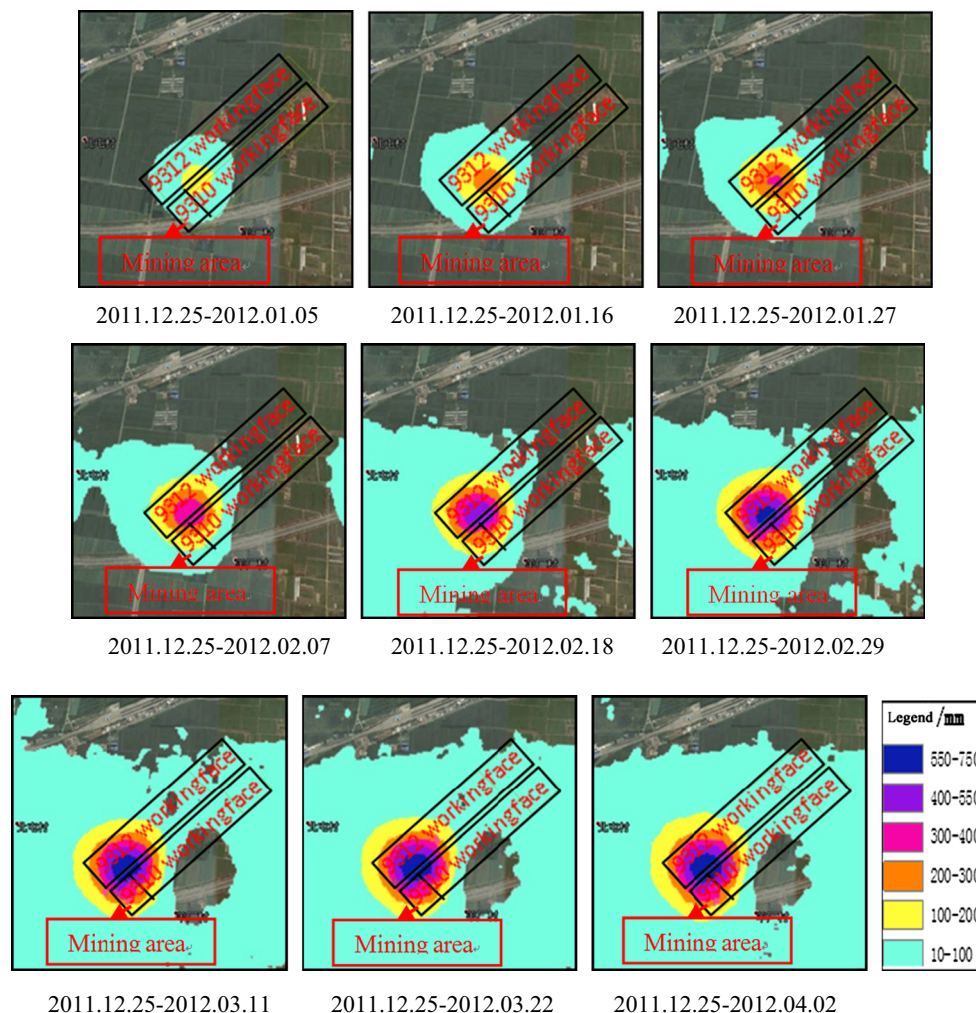
Figure 6 shows the changing process of surface subsidence and subsidence value in the excavation area of the 9210 working face in 2012. The maximum surface subsidence monitored by SAR images is not in the central section of the working face, and surface subsidence of the 9310 working face moves towards the abandoned goaf of the 9312 face. The dip angle of the upper coal seam of the No. 3 seam (9310 working face) is 9° and does not appear to affect surface subsidence distribution significantly. Instead, the surface subsidence basin displacement is influenced by the abandoned goaf.

Considering that surface subsidence remains approximately concentric around the maximum surface subsidence, the surface subsidence basin displacement is defined as the projected distance of the maximum subsidence to the center of the mining area in a vertical direction between the working face and abandoned goaf. The surface subsidence basin displacement of the 9310 working face is 34.08 m; this is because it is only 20 m from the 9310 working face to the abandoned goaf, and the working face mining may have caused instability in the central partition coal pillars and masonry beam structure on the boundary of the abandoned goaf.

Table 2 Parameters of the interference images

Sequence numbers	Date		Baseline time/day	Baseline offset/m
	Main image	Secondary image		
1	2011.12.25	2012.01.05	11	−15
2	2012.01.05	2012.01.16	11	105
3	2012.01.16	2012.01.27	11	6
4	2012.01.27	2012.02.07	11	90
5	2012.02.07	2012.02.18	11	−141
6	2012.02.18	2012.02.29	11	144
7	2012.02.29	2012.03.11	11	163
8	2012.03.11	2012.03.22	11	138
9	2012.03.22	2012.04.02	11	−92

Fig. 6 Time series deformation maps of the 9312 and 9310 working faces

2011.12.25-2012.01.05   2011.12.25-2012.01.16   2011.12.25-2012.01.27

2011.12.25-2012.02.07   2011.12.25-2012.02.18   2011.12.25-2012.02.29

2011.12.25-2012.03.11   2011.12.25-2012.03.22   2011.12.25-2012.04.02

Influence of the abandoned goaf on surface subsidence distribution

Computing technology and modern mechanics theory can be used to comprehensively model the mine's geological conditions by numerical simulation. This method has been widely used to study overlying strata movement in coal mining (Yu et al. 2007; Shi and Liu 2008), and in this paper, numerical simulation is adopted to further study the influence of the abandoned goaf on the distribution of the surface subsidence basin.

Numerical model establishment

From Table 3 it is evident that the distribution of strata has been obtained, and the coal seams are flat-lying. From this base model, FLAC®3D (Itasca™ Consulting Group, Minneapolis, MN, USA) was used to establish the numerical model (Fig. 7). The rock mechanical parameters were determined by inversion of the measured data. The resulting model is 2000 m long, 1200 m wide and 299 m

high; the height differs slightly from the height of the rock strata. The plane view size of the model grid is 50×40 m, and there are 28,000 units with 50,184 nodes. The bottom boundary of the model was fully constrained where $u = v = 0$ (u = displacement in the x-direction and v = displacement in the y-direction), while the top has a free boundary. The left and right boundaries were constrained by horizontal displacement, and the constitutive model of rock numerical simulation uses the Mohr–Coulomb method.

It can be noted that the intensity of caving and fracture zones is greatly reduced after fracturing in terms of rock mass destruction during mining subsidence. Thus, while Mahdi and Charlie (2012) indicated that simulation is more reasonable and reliable for a rock mass in a fissure zone when strain softening is applied, it is not reasonable to ignore the intensity change process of a rock mass. According to the computed results by empirical formula and the actual strata, the constitutive models between the conglomerates and coal seams are set as strain softening models, and the rock mass and soil mass above the

Fig. 7 Numerical model
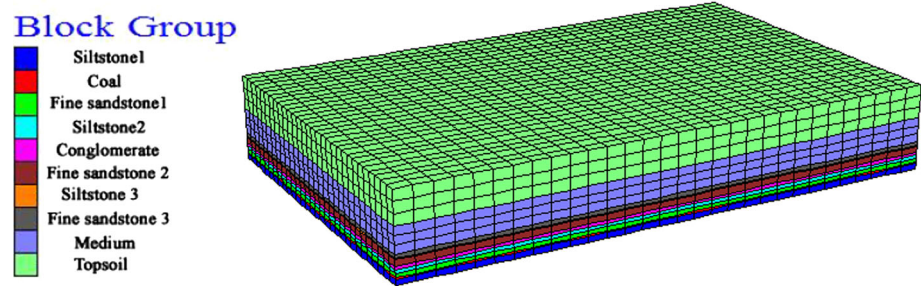
Table 3 Strata distribution and structural parameters of the numerical simulation

Lithology	Elasticity modulus (GPa)	Poisson ratio	Tensile strength (MPa)	Cohesion (MPa)	Internal friction angle (°)	Thickness (m)	Model height (m)
Siltstone	8.45	0.25	0.425	1.89	29.5	20	20
Coal	1.46	0.3	0.5	0.5	30	5	25
Fine sandstone	3.55	0.22	0.775	2.01	34	14	39
Siltstone	8.45	0.25	0.425	1.89	29.5	11	50
Conglomerate	16.75	0.29	1.94	5.7	32	10	60
Fine sandstone	3.55	0.22	0.775	2.01	34	13	98
Medium	5.15	0.26	0.69	2.61	37.2	86	184
Topsoil	0.8	0.35	0.05	0.15	20	115	299

conglomerates are set according to the Mohr–Coulomb method. Elastic plastic slipping contact interfaces are set between different strata to simulate the bedded sedimentary characteristics of the coal and rock mass.

Reliability analysis of the numerical model

The modeled excavation areas are the 9312 and 9310 working faces, but we have focused on the effects of the 9312 abandoned goaf on displacement of the 9310 working face subsidence in 2012. The strata were assumed to be stable during excavation of the 9310 working face in 2012, and the mining area was not affected by other working faces. When conducting the numerical simulation, the displacement was cleared to zero before the mining of the 9310 face in 2012; the initial numerical simulation results are shown in Fig. 8.

As seen in Fig. 8, the simulated surface subsidence basin of the 9310 working face slopes toward the goaf of 9312, and the maximum surface subsidence is not in the center of the mining area. The central zone of simulated subsidence distribution is similar to that of the InSAR monitoring, indicating that the established model agrees with reality. The maximum surface subsidence value is less than the measured data because the effect of mining in 2011 on the 9310 face was not considered.

Relation of basin displacement to the abandoned goaf

From mechanical analysis and InSAR monitoring results, it is evident that surface subsidence basin displacement above the working face is related to the width of the goaf and its distance from the working face. To study this relationship further, the excavation width of the abandoned goaf was set at different intervals of 100, 150, and 200 m, and the distance between mining area and abandoned goaf was set at 50, 150, and 200 m. By extracting and processing the simulated results, the relationship can be graphically shown (Fig. 9).

As seen in Fig. 9, the offset value of the working face surface subsidence basin is related to the width of the abandoned goaf. The offset value of the surface subsidence basin initially increases with an increase in width of the abandoned goaf, and then gradually decreases to stabilization. Thus, there is a critical value for the distribution of the surface subsidence basin above the adjacent working face; when the width of the abandoned goaf reaches this critical value, the pressure on the middle strata is relatively stable. Even though the width of the abandoned goaf increases, the compaction of the middle caving strata reaches a maximum and does not cause secondary subsidence. At the same time, the relationship between the offset

Fig. 8 Comparison between numerical simulation results and SAR monitoring results of surface subsidence
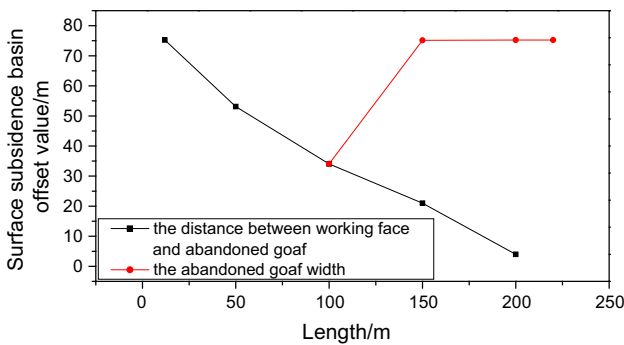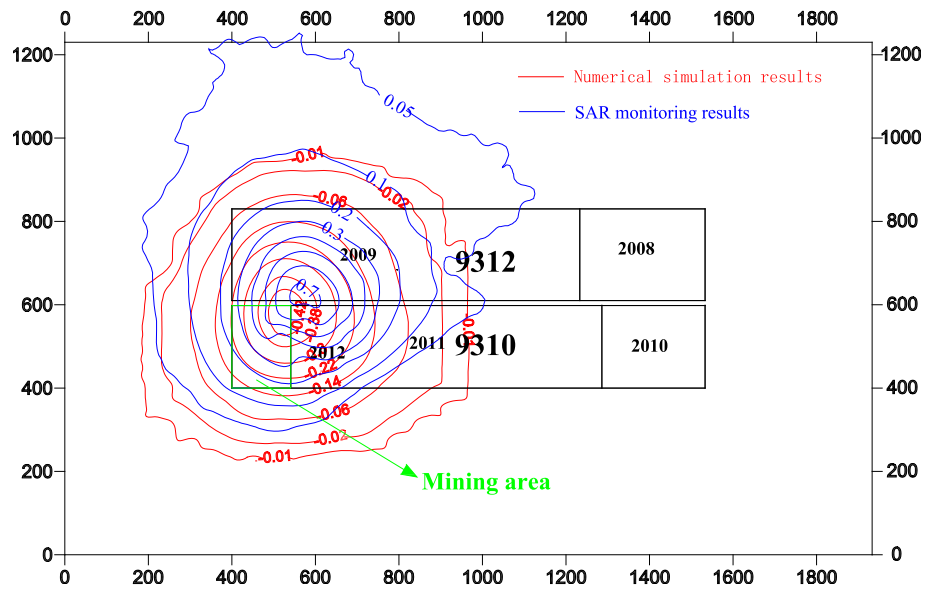

Fig. 9 Graphical representation of the relationship between the offset of the surface subsidence basin and the abandoned goaf width and the distance between the working face and abandoned goaf

of the surface subsidence basin and the distance from the working face to the old gob area can be obtained by data fitting, as shown in Fig. 7.

As shown in Eq. 3, the relationship between these parameters is linear, with a degree of fit (r^2) of 0.97. As the distance between the working face and the old gob increases, the offset value of the surface subsidence basin decreases.

$$y = -0.374x + 76.384. \tag{3}$$

Case study

Predictive modeling using the probability integral method

Currently, probability integration modeling is the main predictive method of modeling strip mining, and its

reliability has been demonstrated over many years of engineering practice. The basic principles of the model (He et al. 1991) are presented below in five key steps, as follows:

1. The surface subsidence value $W(x, y)$ at any point $A(x, y)$ is calculated as shown below in Eq. 4:

$$W(x, y) = W_{cm} C'_x C'_y \tag{4}$$

   in which the values of C'_x and C'_y (the subsidence distribution coefficients of the projection point for an unknown point along strike and dip, respectively) are derived from Eq. 5:

$$\begin{cases} C'_x = \dfrac{1}{\sqrt{\pi}} \left(\displaystyle\int_0^{\frac{x\sqrt{\pi}}{r}} e^{-\lambda^2} \cdot \mathrm{d}\lambda - \int_0^{\frac{(x-L)\sqrt{\pi}}{r}} e^{-\lambda^2} \cdot \mathrm{d}\lambda \right) \\ C'_y = \dfrac{1}{\sqrt{\pi}} \left(\displaystyle\int_0^{\frac{y\frac{x\sqrt{\pi}}{r}}{}} e^{-\lambda^2} \cdot \mathrm{d}\lambda - \int_0^{\frac{(y-1)\sqrt{\pi}}{r}} e^{-\lambda^2} \cdot \mathrm{d}\lambda \right) \end{cases}, \tag{5}$$

   where W_{cm} is the maximum surface subsidence value of full mining ($W_{cm} = mq\cos\alpha$), m is the mining coal seam thickness, q is the surface subsidence coefficient, α is the coal seam dip angle, and L and l are the calculated mining width on the surface along the tendency direction and mining length along the strike direction after translation of the mining inflection points, respectively. The factors r, r_1 and r_2 are the major influencing radii of the strike, downhill and uphill directions, respectively, and x and y are the unknown point coordinates.

2. The surface tilted deformation value $T(x, y)_\varphi$ at any point $A(x, y)$ along the φ direction is calculated as shown below in Eq. 6:

$$\begin{cases} T(x,y)_\varphi = T_x C_y' \cos\varphi + T_y C_x' \sin\varphi \\ T(x,y)_{\varphi+90} = -T_x C_y' \sin\varphi - T_y C_x' \cos\varphi, \\ T(x,y)_m = T_x C_y' \cos\varphi_T + T_y C_x' \sin\varphi_T \end{cases} \quad (6)$$

where φ_T is the angle between the maximum tilt direction and the OX axis (counter-clockwise rotation) and $\varphi_T = arctg(T_y C_x'/T_x C_y')$. The factor $T(x, y)_m$

where φ_u is the angle between the maximum horizontal movement direction and the OX axis. This angle is calculated as $\varphi_u = arctg(U_y C_x'/U_x C_y')$. The factors U_x and U_y are, respectively, the horizontal movement value of the unknown point along the strike, and the tendency direction in the main section after superimposing the value of the projection point.

5. Finally, the surface horizontal deformation value $\varepsilon(x, y)_\varphi$ at any point $A(x, y)$ along the φ direction is calculated as shown below in Eq. 9.

$$\begin{cases} \varepsilon(x,y)_\varphi = \varepsilon_x C_y' \cos^2\varphi + \varepsilon_y C_x' \sin^2\varphi + \left[(U_x T_y + U_y T_x)/W_{cm}\right] \cdot \sin\varphi \cdot \cos\varphi \\ \varepsilon(x,y)_{\varphi+90} = \varepsilon_x C_y' \sin^2\varphi + \varepsilon_y C_x' \cos^2\varphi - \left[(U_x T_y + U_y T_x)/W_{cm}\right] \cdot \sin\varphi \cdot \cos\varphi \\ \varepsilon(x,y)_{max} = \varepsilon_x C_y' \cos^2\varphi_\varepsilon + \varepsilon_y C_x' \sin^2\varphi_\varepsilon + \left[(U_x T_y + U_y T_x)/W_{cm}\right] \cdot \sin\varphi_\varepsilon \cdot \cos\varphi_\varepsilon \\ \varepsilon(x,y)_{min} = \varepsilon(x,y)_\varphi + \varepsilon(x,y)_{\varphi+90} - \varepsilon(x,y)_{max} \end{cases} \quad (9)$$

is the maximum tilt value of the unknown point in mm/m, and T_x and T_y are, respectively, the tilt deformation values of an unknown point along strike, and the tendency direction in the main section after superimposing the value of the projection point in mm/m.

3. The surface curvature deformation $K(x, y)_\varphi$ at any point $A(x, y)$ along the φ direction is calculated as shown below in Eq. 7:

$$\begin{cases} K(x,y)_\varphi = K_x C_y' \cos^2\varphi + K_y C_x' \sin^2\varphi + (T_x T_y/W_{cm})\sin 2\varphi \\ K(x,y)_{\varphi+90} = K_x C_y' \sin^2\varphi + K_y C_x' \cos^2\varphi - (T_x T_y/W_{cm})\sin 2\varphi \\ K(x,y)_{max} = K_x C_y' \cos^2\varphi + K_y C_x' \sin^2\varphi - (T_x T_y/W_{cm})\sin 2\varphi_k \\ K(x,y)_{min} = K(x,y)_\varphi + K(x,y)_{\varphi+90} - K(x,y)_{max} \end{cases} \quad (7)$$

where: $\varphi_k = \frac{1}{2}arctg\frac{2T_x T_y}{W_{cm}(K_x C_y' - K_y C_x')}$ and $K(x, y)_{max}$ and $K(x, y)_{min}$ are the maximum and minimum curvature deformation values of the unknown point, respectively. The factors K_x and K_y are, respectively, the curvature values of an unknown point along the strike and the tendency direction in the main section after superimposing the value of the projection point.

4. The surface horizontal movement value $U(x, y)_\varphi$ at any point $A(x, y)$ along the φ direction is calculated as shown below in Eq. 8:

$$\begin{cases} U(x,y)_\varphi = U_x C_y' \cos\varphi + U_y C_x' \sin\varphi \\ U(x,y)_{\varphi+90} = -U_x C_y' \cos\varphi + U_y C_x' \sin\varphi, \\ U(x,y)_{cm} = -U_x C_y' \sin\varphi_u + U_y C_x' \cos\varphi_u \end{cases} \quad (8)$$

where: $\varphi_\varepsilon = \frac{1}{2}arctg\frac{U_x T_y + U_y T_x}{W_{cm}(\varepsilon_x C_y' - \varepsilon_y C_x')}$ and $\varepsilon(x, y)_{max}$ and $\varepsilon(x, y)_{min}$ are the maximum and minimum horizontal deformation values of the unknown point, respectively. The factors ε_x and ε_y are, respectively, the horizontal deformation values of the unknown point along strike, and the tendency direction in the main section after superimposing the value of the projection point.
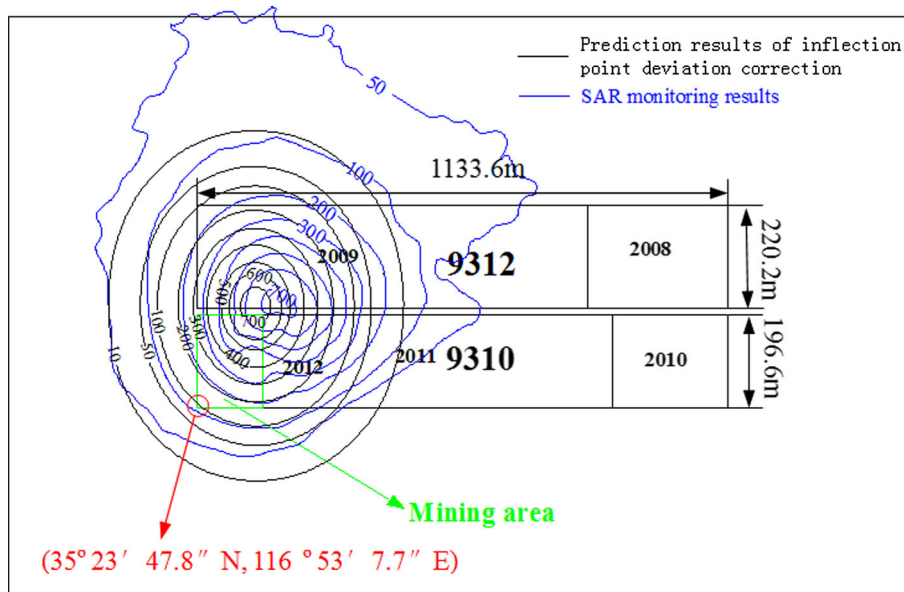
Selecting inflection point deviation

When the probability integral method is used to predict the distribution of the surface subsidence basin influenced by the abandoned goaf, it is generally done by amending the inflection point deviation in the direction of the abandoned goaf, i.e., by changing the values of l and L in Eq. 5. The inflection point deviation is set to zero or the opposite of the initial value, and other prediction parameters remain unchanged.

The predicted result is that the surface subsidence basin moves in the direction of the abandoned goaf, and it is evident that the value of inflection point deviation is related to the offset value of the surface subsidence basin. Analysis of the simulated results shows that the offset value of surface subsidence is related to the width of the abandoned goaf and the distance between the working face and abandoned goaf. It is therefore not reasonable to set the deviation of the inflection point to zero or the opposite value of the initial value.

Thus, the distance between the working face and abandoned goaf, and the width of the abandoned goaf, should be considered comprehensively to select the

Fig. 10 Comparison between the predicted results of inflection point deviation correction and the SAR monitoring results

inflection point deviation in the direction of the abandoned goaf when using the probability integral method. The choice of the inflection point deviation should decrease with increasing distance between the working face and abandoned goaf, and should first increase and then gradually stabilize with increasing width of the abandoned goaf. A comparison between the surface subsidence basin results obtained from the probability integral method and the SAR image monitoring results is shown in Fig. 10. The predicted central zone distribution of the surface subsidence basin is consistent with the distribution of SAR image monitoring, which verifies the probability integral analysis.

Conclusions

1. The main effect of an abandoned goaf on the surface subsidence basin offset is that excavation causes a link to develop between the void region and the under-compacted area of the abandoned goaf. The mining-induced additional stress from the adjacent working face is also important, as it causes further compaction of the fractured rock mass in the middle of the abandoned goaf.

2. D-InSAR technology is effective in monitoring the full and dynamic changes that affect the surface subsidence basin. The results show that the surface subsidence basin will become displaced under the influence of the abandoned goaf.

3. The offset value of the surface subsidence basin is related to the width of the adjacent abandoned goaf and the distance between the working face and abandoned goaf. If the width of the abandoned goaf increases, the offset value of surface subsidence initially increases and then gradually stabilizes. The offset value of surface subsidence declines with increasing distance between the working face and abandoned goaf; with increasing distance, the offset value of surface subsidence initially decreases exponentially and then decreases linearly.

4. In practice, the distance between the working face and abandoned goaf, and the width of the abandoned goaf, should be considered comprehensively when selecting inflection point deviation in the direction of the abandoned goaf. Absolute values can be fixed by the data, as shown in Fig. 6, or by numerical simulation. Numerical simulation is a promising method for future research into the distribution of surface subsidence basins and movement of overlying strata caused by the interaction of multiple working faces.

References

Baryakh AA, Telegina EA, Samodelkina NA et al (2005) Prediction of the intensive surface subsidences in mining potash series. J Min Sci 41(4):312–319

Fan HD (2010) Study on several key algorithms of InSAR technique and its application in land subsidence monitoring. China University of Mining Technology, Xuzhou

Gabriel AK, Goldstein RM, Zebker HA (1989) Mapping small elevation changes over large areas: differential radar interferometry. J Geophys Res Solid Earth 94(B7):9183–9191

Gu SC, Hong X (2012) Application of probability integral method in mountainous area surface movement prediction with shallow coal seam. J Xi'an Univ Sci Technol 32(1):45–50

Gu Y, Song ZH, Zhang SW (2011) Research of mining settlement estimate based on probability integration. J Shandong Univ Technol 25(1):33–36

Guo ZZ, Xie HP, Wang JZ (2004) Applying probability distribution density function to predict the surface subsidence caused by subcritical extraction. J China Coal Soc 29(2):155–158

Guo G, Zhu X, Zha J et al (2014) Subsidence prediction method based on equivalent mining height theory for solid backfilling mining. Trans Nonferrous Metals Soc China 24(10):3302–3308

He GQ, Ling GD, Yang L (1991) Mining subsidence. China University Mining Technology Press, Xuzhou **(in Chinese)**

Li CL, Xie MW, Li XL (2007) GIS and probability integral based approach for subsidence prediction and application to beiminghe iron mine. Chin J Rock Mech Eng 26(6):1243–1250

Li HZ, Guo GL, Zha JF, Yuan YF, Zhao BC (2015) Research on the surface movement rules and prediction method of underground coal gasification. Bull Eng Geol Environ. doi:10.1007/s10064-015-0809-7

Liu YC, Cao SG (2012) Preliminary study of surface subsidence model based on theory of key rock stratum. Rock Soil Mech 03:719–724

Liu BC, Liao GH (1965) The basic rule of surface movement in coal mine. China Industrial Press, Beijing

Mahdi S, Charlie C (2012) Numerical modeling of longwall mining and stability analysis of the gates in a coal mine. Int Rock Mech Min Sci 51:24–34

Nicieza CG, Fernández MIÁ, Díaz AM et al (2005) The new three-dimensional subsidence influence function denoted by n–k–g. Int J Rock Mech Min Sci 42(3):372–387

Nie L, Wang H, Xu Y et al (2015) A new prediction model for mining subsidence deformation: the arc tangent function model. Nat Hazards 75(3):2185–2198

Shi BM, Liu ZG (2008) Numerical simulation of the upper coal and rock deformation characteristic caused by mining protecting stratum. J China Coal Soc 01:17–22

Soni AK, Singh KKK, Prakash A et al (2007) Shallow cover over coal mining: a case study of subsidence at Kamptee Colliery, Nagpur, India. Bull Eng Geol Environ 66(3):311–318

Wu SC, He YG, Xu P (2010) Probability integral method for the prediction of surface deformation of mined-out area beneath a highway. Safe Environ Eng 17(5):119–122

Yang MZ, Ren XF, Yu YX (2007) Application of probability integration to dynamic appraisal of surface distortion in coal depletion region. J Xi'an Univ Sci Technol 27(1):39–42

Yang Y, Gong ZQ, Liang B (2011) Dynamic subsidence basins in coal mines based on rock mass rheological theory. Int J Min Sci Technol 21:333–335

Yin SX, Yu XY, Hu QH (2010) Application of curved surface fitting technology in mining subsidence prediction. J Xi'an Univ Sci Technol 30(5):518–522

Yu BH, Zhu WB, Xu JL (2007) Numerical simulation of surface subsidence induced by deep mining. J Min Saf Eng 04:422–426

Zebker HA, Goldstein RM (1986) The displacement field of the landers earthquake mapped by radar interferometry. J Geophys Res 91:4993–4999

Zhang LG (2009) Overburden failure mechanism and surface movement law due to sub-critical extraction in Yangzhou mining area. China University Mining Technology, Xuzhou